Received: 2 June 2023 | Revised: 27 November 2023 | Accepted: 8 December 2023
DOI: 10.1002/esp.5763

RESEARCH ARTICLE

ESPL WILEY

Using additional roughness to characterize erosion control treatment effectiveness in roadside ditch lines

Amanda D. Alvis[1] | Charles H. Luce[2] | Erkan Istanbulluoglu[1] | Thomas Black[2] | Julie Dieu[3] | Jenelle Black[4]

[1]Department of Civil and Environmental Engineering, University of Washington, Seattle, Washington, USA
[2]Rocky Mountain Research Station, USDA Forest Service, Boise, Idaho, USA
[3]Pacific Resource Unit, Rayonier, Hoquiam, Washington, USA
[4]CMER Science Staff, Northwest Indian Fisheries Commission, Olympia, Washington, USA

Correspondence
Amanda D. Alvis, Department of Civil and Environmental Engineering, University of Washington, Seattle, WA, USA.
Email: amanaste@uw.edu

Funding information
Cooperative Monitoring, Evaluation, and Research (CMER) Committee within the Washington State Department of Natural Resources Adaptive Management Program

Abstract
Forest roadside ditch lines capture and redirect road runoff and typically have erosion control treatments installed therein. Existing methods used to determine the effectiveness of roadside ditch line erosion control treatments estimate fixed fractional reductions in sediment yield. However, fixed fractional reductions do not describe dependence on any measurable physical property of treatment, climate, and the environment. Here, we use additional flow roughness induced by erosion control treatments as a metric that can be used as the basis of estimating treatment effectiveness in varying contexts. We investigate its utility in small-scale field experiments in western Washington. We measured the physical characteristics of each ditch (e.g., shape, soil texture, and slope) and flow velocities and sediment concentrations for each treatment under multiple experimental discharges. We then used the concept of shear stress partitioning to relate sediment yield from the ditch line erosion treatments to grain shear stress, which is a function of flow roughness (Manning's n) of the respective treatment. We found that (1) a given erosion control treatment produced consistent Manning's n values across multiple replications and sites, with a bare ditch (no treatment) yielding the lowest roughness ($n = 0.05$) and a densely wattled ditch yielding the highest roughness ($n = 0.75$); (2) sediment load and calculated grain shear stress data yielded a single positive relationship when data from each experiment were combined, which suggests the effect of additional roughness on grain shear stress is a main driver in the reduction of ditch line sediment load; and (3) in our dataset, fractional erosion reduction had a variable and nonlinear sensitivity to low flow rates (99% of observed flows) for lower roughnesses. Our results demonstrate how additional flow roughness can be used as a general metric to help evaluate the effectiveness of ditch line erosion control treatments for a variety of physical conditions.

KEYWORDS
erosion, erosion control treatments, forest roads, hydrology, sediment transport, shear stress

1 | INTRODUCTION

Roadside ditch lines are crucial conduits for capturing and redirecting forest road runoff to mitigate the effects of forest road erosion. Erosion control treatments for dirt and gravel roads—especially those that are installed in roadside ditch lines—are essential to the protection of both transportation infrastructure and downstream water quality and aquatic habitat (e.g., Cristan et al., 2016). Accurate estimates of erosion reduction from forest road surfaces and ditch lines are critical to developing regulations and assessing the cost effectiveness of erosion control treatments (e.g., wattles, gravel, and vegetation; see, e.g., Boston, 2016; Dangle et al., 2019). Most of the current research evaluating the efficacy of these treatments has been done in the vein of randomized control trials (sensu Cartwright, 2007) and relies on empirical methods that quantify a fixed fractional reduction of sediment transport (e.g., Aust et al., 2015; Burroughs et al., 1984; Burroughs & King, 1989; Cristan et al., 2019; Edwards et al., 2016; Luce & Black, 1999; Megahan, 1974; Megahan et al., 2001). The choice to use randomized control trials—rather than developing physics-based models and testing those models using experiments—is likely driven by a few key factors. For one, each erosion control treatment involves distinct mechanisms for reducing ditch line erosion. Rather than focussing on details of different process representations in models, empirical field methods can be used to determine reduction factors. Additionally, multiple treatments are commonly used within a single project to assess their efficacy, and the interactions among these treatments pose challenges for modelling due to their complex nature. Finally, a large portion of the motivation behind this research originates from practitioners rather than academics. Practitioners have preferred methods that can be easily implemented without the need for vast data collection and site characterization.

A major challenge in using fixed fractional reductions in erosion is in the generalization of the effects of the erosion control treatments to other contextual settings. For example, the fixed fractional reduction in sediment estimated from an experiment conducted in a place where high intensity rainstorms occur may not apply in places where snow melt generated runoff is more common. The results that are calculated from an experiment on a steep road will likely not be equivalent to those of a low-gradient road. The general applicability of limited experimental results to a wide range of ditch conditions and treatments is hindered by the presence of thresholds and nonlinearities in the sediment entrainment and transport process (e.g., Al-Hamdan et al., 2013; Buffington & Montgomery, 1997; Govers, 1992; Nearing et al., 1989). To address the need for erosion predictions in a wide range of field conditions, differences in experimental controls or premises need to be accounted for in the development of models and/or methods. These differences can be considered either through conducting more randomized control trials in various experimental settings (a potentially slow and expensive process) or through a more process-based approach, where a simple physical parameter is used. We advocate for the latter by proposing to use additional roughness imparted by different ditch line erosion treatments as that simple physical parameter. Additional flow roughness is the increment in roughness affecting flowing water caused by placement or growth of materials/vegetation in the ditch. We then partition the shear stress acting on the water column between particles on the bed versus the added roughness elements. The concept of shear stress partitioning is a well-known method in sediment transport literature to represent how additional flow roughness elements on the bed reduce the shear stress acting on sediment particles (Einstein & Banks, 1950; Einstein & Barbarossa, 1952).

In practice, three main mechanisms help erosion control treatments reduce sediment transport and erosion in ditch lines: (1) increasing flow roughness, (2) binding, and (3) filtering. Increasing the roughness of the flow by placing additional roughness elements, such as grass and wattles, to slow down the flow velocity is well-grounded in observational evidence (e.g., Donald et al., 2013; Edwards et al., 2016; Li et al., 2020; Li, Zhang, et al., 2022; Prosser et al., 1995; Schussler et al., 2021; Whitman et al., 2021). Other erosion control treatments approach erosion reduction through binding and filtering, both of which may involve additional physical mechanisms that decrease the erodibility of the bed material or reduce erosivity of flows. Binding refers to treatments that functionally increase the size of particles that would need to be transported. Examples of binding treatments include concrete lining, maintaining vegetative root mats, or spreading a binding agent (e.g., Edwards et al., 2016; Likitlersuang et al., 2020; Sojka et al., 2007). Filtering treatments seek to capture particles that are in transport by passing them through some kind of sieving or settling element along a flow path. Examples of filtering treatments include constructed wetlands, straw bales, and rock check dams (e.g., Collins & Johnston, 1995; Edwards et al., 2016; Tollner et al., 1977; Wright, 2010). In the context of controlling erosion in the roadside ditches of rural and forest roads, most common treatments combine two or more of these effects to some degree. Not all erosion control treatments utilize binding and/or filtering, but all treatments do impart some degree of additional flow roughness, which affects shear stress partitioning. As a result, investigating the role of additional roughness—and therefore that of shear stress—on flow and sediment loads is a logical first step towards developing process-based modelling tools and conceptual frameworks to interpret field observations. Shear stress partitioning is a well-established method in the soil erosion literature of rangelands, landscape evolution, and fluvial geomorphology (e.g., Al-Hamdan et al., 2022; Darby et al., 2010; Foster et al., 1989; Istanbulluoglu et al., 2002, 2003; Li, Venditti, et al., 2022; Yager et al., 2007; Yetemen et al., 2019). However, such a method has not seen much attention in erosion control practices literature.

The idea of shear stress partitioning and its theory as developed by multiple researchers, particularly in fluvial environments (e.g., Buffington & Montgomery, 1997; Einstein & Banks, 1950; Einstein & Barbarossa, 1952; Ferguson et al., 2019; Manga & Kirchner, 2000), provides the basis for quantification of changes in total versus effective shear stress on grains with application of different treatments. Increased flow roughness (i.e., the addition of erosion control treatments) leads to deeper flows and thereby higher shear stress or stream power for sediment entrainment and transport. Consequently, a proportion of this shear stress is imparted on the added roughness elements rather than the bed sediment due to increases in friction around the immobile roughness elements. Effectively, the addition of erosion control treatments reduces the shear stress available for the bed, which decreases the frequency and magnitude of sediment mobilization and transport under a variable climate. A substantial body of literature already exists on shear stress partitioning and its effects on sediment transport that supports the use of additional roughness as a metric to determine reduction in sediment mobilization (e.g., Istanbulluoglu & Bras, 2005; Le Bouteiller & Venditti, 2015).

Critically, the roughness contributions from common ditch line erosion control treatments are unknown, and the literature provides scant recommendations to estimate additional flow roughness (i.e., Manning's *n*) contributed by erosion control treatments. Roughness is typically used as a calibration parameter in models (Lane, 2014) and is based on approximate guidelines (e.g., Arcement & Schneider, 1989) offering large ranges in values. However, we posit that incremental roughness added by an erosion control treatment—a simple physical parameter—can be used as a measure or index of erosion control treatment effectiveness. We are left with multiple questions: What is the additional Manning's roughness due to different treatments? What is the influence of increased roughness on sediment load? Is increasing additional flow roughness the dominant mechanism for reducing sediment yields in select roadside ditch line erosion control treatments? Can additional flow roughness be used as a simple physical metric to generalize the effects of the treatments to other contextual settings?

In this paper, we examine several ditch line erosion control treatments through estimating their added roughness as well as measuring sediment transport in field experiments in western Washington. Using these measurements, as well as established theory around shear stress partitioning, we evaluate the utility of roughness as a quantitative characterization of ditch line erosion control treatments. Overall, this study offers potential simplification of determining erosion control treatment effectiveness through the leveraging of theory in hydraulics and sediment transport to reduce the dimensionality of the experimental measurements.

2 | MATHEMATICAL THEORY

2.1 | Shear stress partitioning

Sediment transport has been related to grain shear stress τ_g (the shear stress acting on sediment grains) in excess of critical shear stress τ_c (the shear stress threshold at which sediment will begin to move) in a power-function form:

$$Q_s \sim (\tau_g - \tau_c)^m. \tag{1}$$

When there are other obstructions in the channel aside from the substrate grains, the portion of shear stress acting on the sediment grains is responsible for transport. A shear stress partitioning ratio, f_g, can be used to determine this portion of the total boundary shear stress that acts on the channel bed substrate grains (e.g., Tiscareno-Lopez et al., 1994).

$$\tau_g = \tau_t * f_g. \tag{2}$$

Einstein and Barbarossa (1952) proposed to partition τ_t into various components such as τ_g and τ_a:

$$\tau_t = \tau_g + \tau_a, \tag{3}$$

where τ_a is the shear stress acting on additional roughness in the channel (e.g., bed forms and vegetation). We write the total shear stress based on a force-balance derivation and equate it to the sum of drag forces acting on grains and additional roughness components (Manga & Kirchner, 2000).

$$\rho_w g R S = \rho_w C_{dg} U^2 + \rho_w C_{da} U^2, \tag{4}$$

where ρ_w is the density of water, g is the acceleration of gravity, R is the hydraulic radius of flow, S is the slope, C_{dg} is the drag coefficient for the sediment grains, C_{da} is the drag coefficient for additional roughness components, and U is the flow velocity. When additional roughness is not present, the equation can be solved for C_{dg}:

$$C_{dg} = \frac{g R_g S}{U^2}, \tag{5}$$

where C_{dg} is assumed to remain constant within the same channel (ditch), even with the addition of any roughness elements. Here, we would like to relate C_{dg} to Manning's n, which is widely used to represent channel roughness in hydraulic engineering applications. If we use Manning's equation for U ($U = \frac{1}{n} R^{2/3} S^{1/2}$), assume parabolic channel geometry, and express R from the equation of parabola, C_{dg} takes the following form (Appendix A):

$$C_{dg} = g n_g^{24/13} Q^{-2/13} S^{1/13} \left(\frac{6}{a}\right)^{1/13}, \tag{6}$$

where n_g is grain roughness, a is a parabolic shape factor, and Q is channel flow. Following the logic of (3) and (4), the drag coefficient of the bare ditch can be added to the drag coefficient for added roughness elements to obtain a total drag coefficient (i.e., $C_{dg} + C_{da} = C_{dt}$). As such, we can write an equation for the total drag coefficient in a similar form:

$$C_{dt} = g n_t^{24/13} Q^{-2/13} S^{1/13} \left(\frac{6}{a}\right)^{1/13}. \tag{7}$$

Substituting (6) and (7) into (4) to write equations for grain and total shear stress, we express the shear stress partitioning ratio in (2) as (8). Upon cancelling the identical terms in the fraction, (8) reduces to (9):

$$f_g = \frac{\tau_g}{\tau_t} = \frac{\rho_w g n_g^{24/13} Q^{-2/13} S^{1/13} \left(\frac{6}{a}\right)^{1/13} U^2}{\rho_w g n_t^{24/13} Q^{-2/13} S^{1/13} \left(\frac{6}{a}\right)^{1/13} U^2}, \tag{8}$$

$$\frac{\tau_g}{\tau_t} = f_g = \left(\frac{n_g}{n_t}\right)^{24/13}. \tag{9}$$

In Appendix A, we show several methods for characterizing flow hydraulics in parabolic channels and derive variations of (9) with the exponent in the shears stress partitioning ratio ranging from 3/2 to 15/8 (1.5 to 1.875).

To obtain the shear stress partitioning ratio, we can characterize n_g from bare ditch lines and n_t from ditch lines with different erosion control treatments. The flow roughness (i.e., Manning's n or Manning's roughness) can be calculated by

$$n = \frac{1}{U} R^{2/3} S^{1/2}. \tag{10}$$

Again, if the channel geometry is assumed to be parabolic, R can be written in terms of other hydraulic and geometric properties (Appendix A), which turns (10) into

$$n = \frac{Q^{4/9} S^{1/2}}{U^{13/9} \left(\frac{6}{a}\right)^{2/9}}. \quad (11)$$

Given fixed Q, S, and a, U becomes the main variable that differentiates the actual roughness values for bare or erosion control treatment conditions, which can then be used in (9). Using (11), Manning's n obtained for a bare ditch gives us n_g, while that which is obtained for ditches with erosion control treatments gives us n_t.

As discussed above, the total shear stress can be divided into various components such as τ_g and τ_a (Equation 3). Combining (3) and (9) and noting that $n_t = n_a + n_g$, we can visualize total shear stress and its division into various components as a function of additional channel roughness, n_a (Figure 1; see also fig. 4 in Manga & Kirchner, 2000, for a related perspective).

2.2 | Transport capacity of ditch flow

To evaluate the reductions of sediment transport of different erosion control treatments relative to bare ditch lines, we use an excess-shear-stress-dependent sediment transport equation developed for rills and overland flow on a noncohesive substrate (Govers, 1992):

$$T_c = \frac{10^{-4.348}}{d_{50}^{0.811}} (\tau_g - \tau_c)^{2.457}, \quad (12)$$

where T_c is the sediment transport capacity of the flow, d_{50} is the median grain size, τ_g is the grain shear stress, and τ_c is the critical shear stress.

2.3 | Indicators of erosion control treatment effectiveness

To examine the effectiveness of erosion control treatments, we look at the contextually determined fractional reduction in grain shear

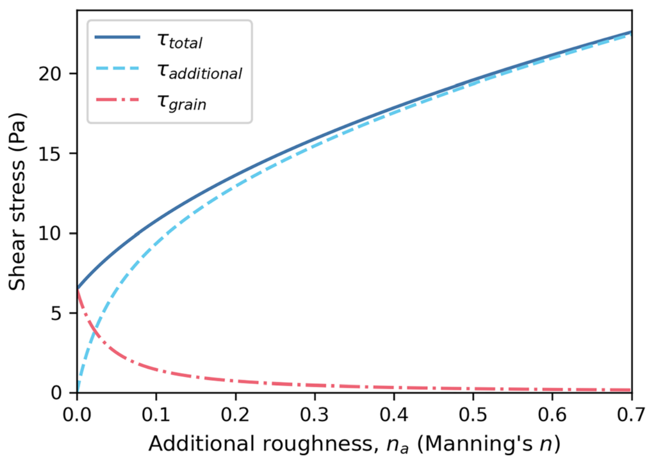

FIGURE 1 The theoretical effect of additional immobile roughness elements on shear stress and its partitioning. [Color figure can be viewed at wileyonlinelibrary.com]

stress and the contextually determined fractional reduction in sediment transport capacity (henceforth referred to in this experiment as "fractional reductions" as opposed to "contextually determined fractional reductions," for clarity). We define the fractional reduction in grain shear stress, ϕ, as

$$\phi = \frac{\tau_{g,bare} - \tau_{g,ect}}{\tau_{g,bare}}, \quad (13)$$

where $\tau_{g,bare}$ is the bed shear stress of a bare ditch, or the shear stress acting on the sediment grains in a bare ditch, and $\tau_{g,ect}$ is the shear stress acting on the sediment grains in a ditch with additional roughness from installed erosion control treatments. This metric allows us to quantify the proportion of reduction of $\tau_{g,bare}$ achieved by an erosion control treatment.

Similar to (13), we define the fractional reduction in sediment transport capacity, θ, as

$$\theta = \frac{T_{c,bare} - T_{c,ect}}{T_{c,bare}}, \quad (14)$$

where $T_{c,bare}$ is the transport capacity of flow in a bare ditch and $T_{c,ect}$ is the transport capacity of flow in a ditch with additional roughness from installed erosion control treatments.

3 | FIELD STUDY

3.1 | Study area

We carried out an experiment to measure the Manning's roughness and sediment load of multiple roadside ditch line erosion control treatments in two regions of southwest Washington state: (1) a volcanic lithology near Mount Saint Helens and (2) a siltstone lithology near Aberdeen, WA. These regions contain multiple field sites with different ditch line treatments, which were selected to be on mainline logging roads as part of a broader study conducted by the Cooperative Monitoring Evaluation and Research Committee within the Washington Department of Natural Resources Adaptive Management Program. Each field site for this experiment consists of a 40 m length of ditch line with a cross-drain culvert at the bottom of the ditch segment and has a slope between 4% and 6% (Figure 2a). The field sites in the volcanic lithology experience, on average, 1560 mm of annual precipitation, and the field sites in the siltstone province experience, on average, 2400 mm of annual precipitation (PRISM Climate Group, 2023), with most of the precipitation occurring between October and April.

The experimental runs were carried out in the volcanic region in May 2021 and May 2022 and in the siltstone region in May 2021, May 2022, and October 2022. In each region, multiple ditch treatments were tested (Table 1 and Figure 2b).

Additionally, in the siltstone region, we performed the same experiment on a rut in the road surface to observe the hydraulic properties of ruts as well as their sediment-carrying effectiveness.

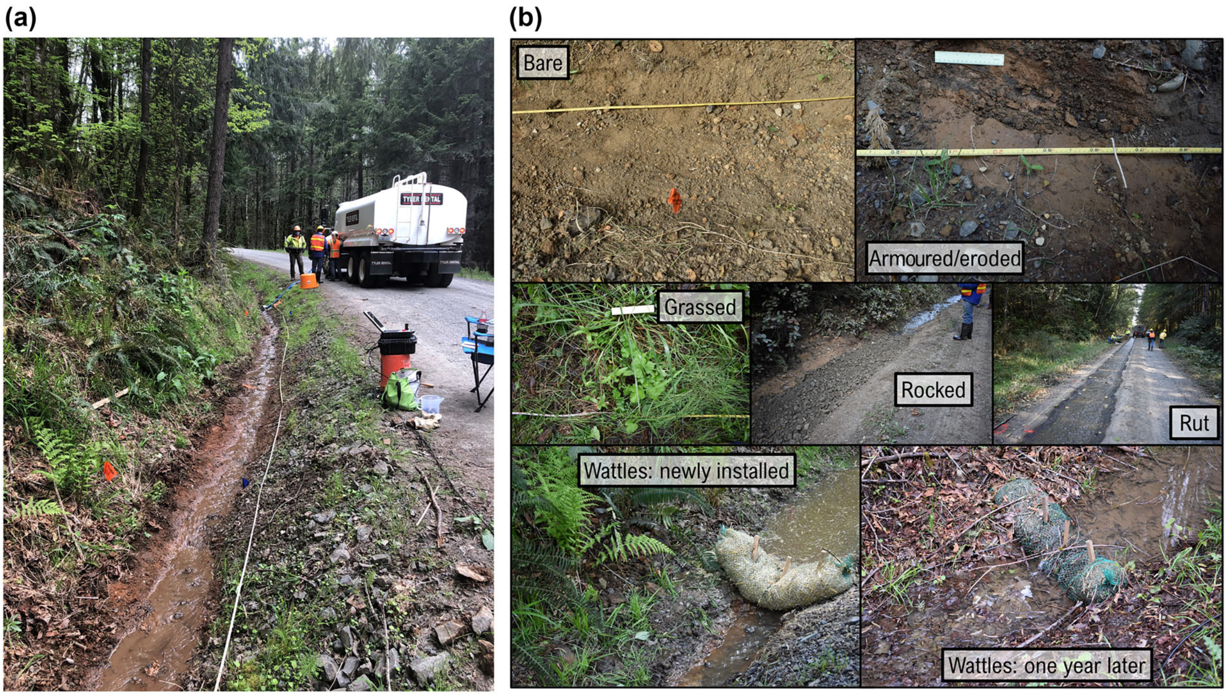

FIGURE 2 (a) Example experimental setup showing the roadside ditch line and water truck and (b) example photos of each ditch line treatment tested. [Color figure can be viewed at wileyonlinelibrary.com]

TABLE 1 Descriptions and locations for each ditch treatment tested.

Treatment	Description	Siltstone region	Volcanic region
Bare subsoil	Freshly ditched and no treatment	x	x
Eroded/armoured	Not recently ditched with minimal grass recovery	x	
Grassed	Not recently ditched with good grass recovery		x
Sparse wattles, initial installation	10 straw wattles		x
Sparse wattles, 1 year post-installation	10 straw wattles		x
Dense wattles, initial installation	19 straw wattles	x	
Rocked	3″ minus rock covering bottom of ditch	x	

3.2 | Experiment

The goal of the experiment was to estimate Manning's roughness and sediment load for each ditch treatment. We examined changes in the hydraulics of flow, as well as sediment production and transport, in roadside ditch lines for multiple roughness-varying erosion control treatments. Each experimental run consisted of the following:

1. Measurements of the physical characteristics of the ditch line (e.g., shape, soil texture, and slope).
2. Collection of surface sediment samples at each of five cross sections (measurement stations) in the ditch.
3. Use of a salt tracer to determine the velocity of flow for three given flow rates (Moore, 2005; United States Bureau of Reclamation, 2001).
4. Collection of sediment samples at the downstream end of the ditch line throughout each experimental run.

We determined the longitudinal profile (i.e., slope) of the ditch using a survey rod and a survey level and established measurement stations at 4 m intervals from the ditch relief cross-drain culvert at the bottom of the ditch segment (origin; 0 m) to the top of the experimental segment (40 m up-ditch). Cross-sectional channel profiles were measured at every other measurement station from the bottom of ditch line (4 m above the pipe inlet and 12, 20, 28, and 36 m) using a level and a metric ruler, with elevation-drop measurements being made at 0.1 m intervals from the cutslope side of the ditch (0 m) to the side of the road (1.1–1.2 m) (Figure 3a).

Sediment was sampled at each of the five cross sections noted above to determine the existing grain size distribution in each experimental ditch. Sediment samples were taken from the surface because the expected transported sediment comes from the surface of the ditch, as flow was provided upstream of each ditch. These samples were originally processed such that we obtained a dispersed grain size distribution. However, because the material in our ditch lines had some cohesion, we took additional samples to obtain a water-stable aggregate grain size distribution for each site following the methods of Kemper and Rosenau (1986). The resulting median grain size was approximately 1 mm, which was used as the median grain size for further analysis (see Section 4). Photographs were taken at each of the

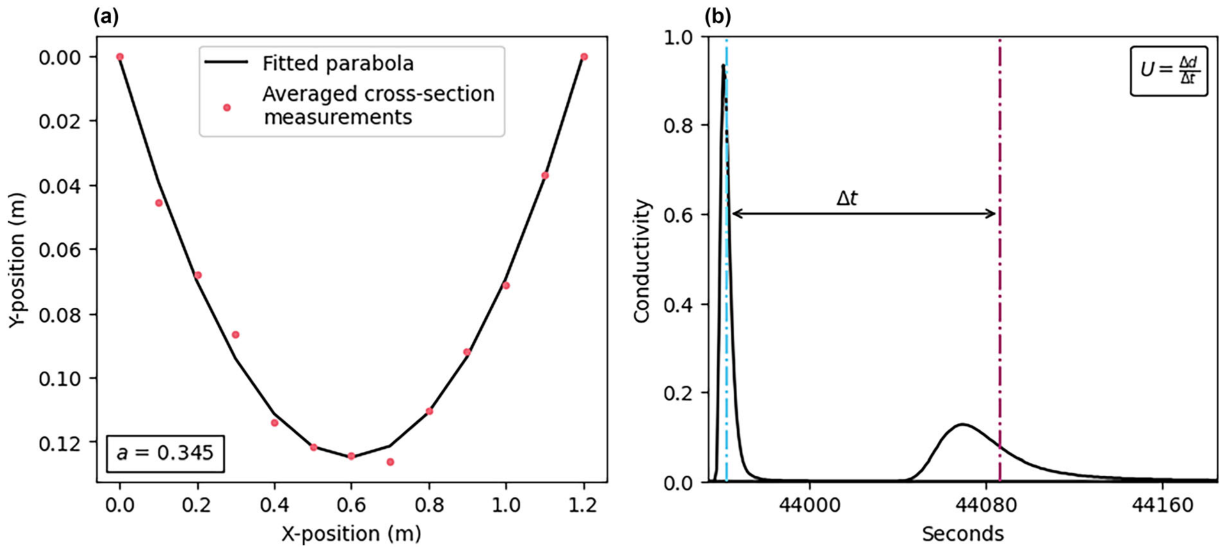

FIGURE 3 Examples of (a) average ditch cross-section measurements with a fitted parabola and shape factor and (b) a conductivity plot for two sensors from the salt tracer experiment. Δt is the time it takes for the salt tracer to get from the upper sensor to the lower sensor (average rate taken as one half area under the curve) and is determined from the plot, and Δd is known. [Color figure can be viewed at wileyonlinelibrary.com]

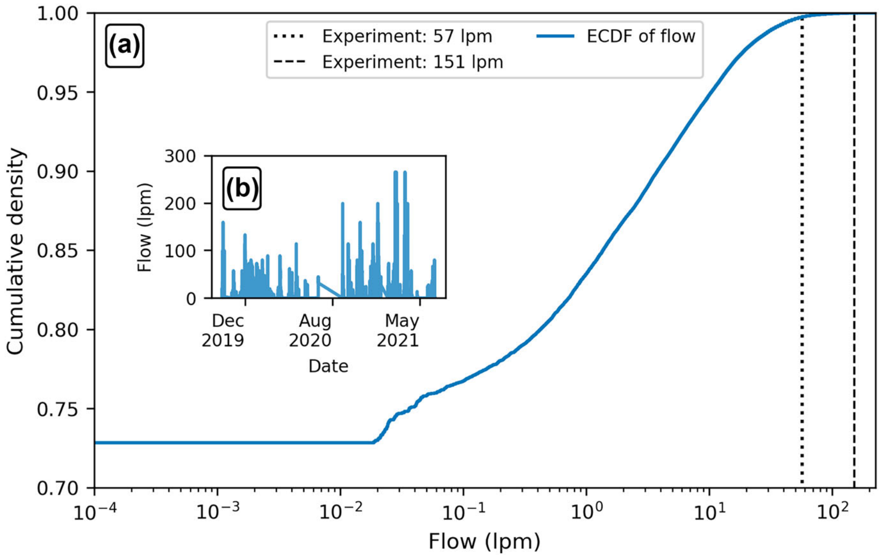

FIGURE 4 (a) Empirical cumulative distribution function (ECDF) of flow data from one of our siltstone lithology field sites in western Washington with vertical lines denoting two of the flows used in the small-scale experiment in litres per minute (57 and 151 lpm). For this site, 57 lpm flows exist in the 99th percentile and 151 lpm flows exist in the 100th percentile. (b) The corresponding tipping bucket flow hydrograph for the 2020 and 2021 water years. [Color figure can be viewed at wileyonlinelibrary.com]

five cross sections noted above to document the physical changes of the ditch line before and after the experimental runs (if any). Finally, to ensure minimal loss of water flow to infiltration during experimental runs, the ditch line was wetted by a water tank truck providing flow at a slow rate (Figure 2a).

To provide known flow rates, we utilized a flow meter (Flomec G2 AI Turbine Flow Meter Model G2A15NQ9GMB) and hose attached at the water tanker outlet. The experimental runs were carried out at three flow rates for each ditch treatment, twice to thrice per flow rate: 57, 95, and 151 L min^{-1} (lpm). These three flow rates were chosen to reflect flows that have been observed in our broader study dataset of these magnitudes. More specifically, these three flow rates exist within the 99th to 100th percentile of empirical flow data recorded at one of our siltstone lithology sites between 2019 and 2021 (Figure 4). Those years experienced slightly drier-than-average climatic conditions (PRISM Climate Group, 2023). We used the high end of the flow rates as most sediment is transported within the wettest few days in ditch lines.

Conductivity probes (Campbell Scientific Model CS547A with a Campbell Scientific CR 1000 Data Logger) were placed in the ditch at just below 4 m and just above 36 m. The conductivity probes measured the passage of salt tracers, used to determine the velocity of the flow during our experimental runs.

Once the flow from the water tank truck stabilized in the ditch line, a known quantity of NaCl was added to the system, signalling the start of the experimental run, and was monitored via conductivity probes. The conductivity probes logged a reading every second. Once the NaCl level for both conductivity probes returned to their original values, the experimental run was considered complete. We repeated the addition of NaCl for each flow and treatment combination twice.

For each experimental run, a grab sample for sediment concentration was collected at the downstream end of the ditch line once the flow rate stabilized. We collected one main sediment concentration sample per run to give us an estimate of sediment transport occurring for each treatment prior to any ditch armouring occurring.

3.3 | Data analysis

In order to calculate Manning's roughness values for each experimental run, we first estimated flow velocities from our salt tracer experiments. We measured the time it takes for the NaCl to travel from the upper sensor to the lower sensor (Figure 3b). With a known distance between the two sensors and the time of travel, we calculated the average velocity of the flow between the two sensors, which is taken as the average velocity for the ditch line flow.

The cross-sectional shape of our ditches for the experimental runs was mostly parabolic (e.g., Figure 3a). Given the estimated U and measured Q, we then characterized the parabolic shape factor, a. To calculate this shape factor, we took the average of the measurements of the ditch line cross-sectional channel profiles and characterized a representative cross-sectional shape of the ditch line. We fit each ditch with an equation for a parabola and estimated the shape factor a.

Given U, Q, a, and the measured mean profile slope of the ditch line, n is obtained from (11). For each erosion control treatment (Figure 2b), we estimated the corresponding n (i.e., n_t) using the steps outlined above. We carried out an ordinary least squares regression analysis to help describe the observed relationship between n_t and flow (Table 2). Ultimately, we were interested in the response of the grain shear stress (i.e., shear stress partitioning) and the sediment transport capacity of the ditch line to additional Manning's roughness, which we calculated based on our measured and calculated experimental values following the logic in Section 2.

In addition to the roughness of each ditch and the grain shear stress of each experimental run, we used our sediment concentration grab samples from each experimental run to corroborate our estimates of shear stress partitioning and sediment transport capacity and test for whether additional factors other than roughness appeared to affect sediment transported along the bottom of the ditch line. Sediment concentrations were converted to sediment transport per unit flow width, which is calculated as $\textit{sediment concentration} * \frac{Q}{w}$ where Q is flow discharge and w is flow width obtained from the parabolic channel cross section assumption at the measured cross-sectional area (Figure 3a).

We used 2 years of measured flow data (1 October 2019–30 September 2021) from one of our field sites to calculate flow durations to be applied (Figure 4) in estimating grain shear stress and sediment transport capacity. This allowed us to address questions about how much of the time sediment might be expected to be produced from the ditch, the expected distribution of sediment export rates, and the fractional reduction in sediment yields as a function of a treatment specified in terms of its added roughness. These flows were used to calculate grain shear stress (τ_g), sediment transport capacity (T_c), the fractional reduction in grain shear stress (ϕ), and the fractional reduction in sediment transport capacity (θ) for different erosion control treatments using their respective Manning's roughness values.

TABLE 2 Statistical analysis results of trend lines shown that relate total roughness and flow.

Treatment	Slope	Coefficient of variance	*P*-value
Dense wattles, initial installation	0.000[a]	1.000[a]	N/A[a]
Grassed	−0.004	0.748	0.026
Sparse wattles, 1 year post-installation	−0.003	0.953	0.003
Sparse wattles, initial installation	0.000	0.021	0.907
Rocked	−0.002	0.890	0.057
Armoured	0.000	0.099	0.319
Bare	0.000	0.405	0.035
Rut	0.000	0.240	0.402

[a]Only two data points.

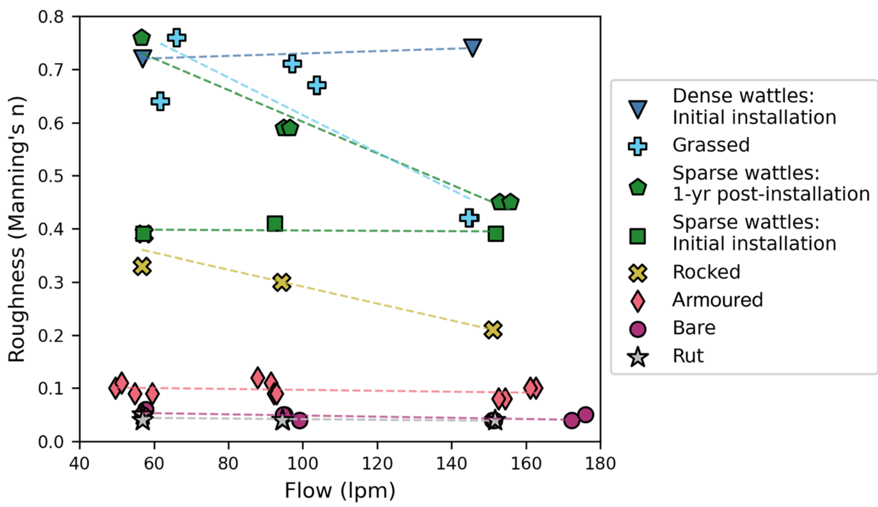

FIGURE 5 Roughness values (Manning's *n*) for each ditch condition and their relationship to flow. [Color figure can be viewed at wileyonlinelibrary.com]

4 | RESULTS

4.1 | Inferences from field observations

To address our first research question, we report estimated total roughness values (Manning's n) from our experiments (Figure 5). Erosion control treatment installation and natural armouring of a ditch line increased n_t as compared with a bare (recently disturbed) ditch. Three erosion control treatments—rocked, grassed, and sparse wattles 1 year post-installation—demonstrated a linearly decreasing relationship between the total roughness and flow (Table 2). Additionally, we performed the same experiment on a heavily defined wheel rut on the road surface (Figure 2b) and found that the rut had similar roughness to a bare (recently disturbed) ditch. The observed increase in Manning's roughness with added erosion control treatments is consistent with the literature and the shear stress partitioning theory, further elaborated in Section 5. The next logical question to address here is as follows: What is the influence of increased roughness on sediment load? We address this question through our sediment concentration data.

Our grab samples provided us with sediment concentration values (Figure 6a) and sediment transport per unit width (Figure 6b) for each treatment and flow. All of our ditch treatments yielded some amount of sediment transport. The bare ditch and rut yielded the highest sediment concentrations and sediment transport, with an armoured ditch yielding at least one order of magnitude less sediment. To provide a more direct comparison, we plot sediment transport from each erosion control treatment staged from low to high n_t, with nominal flow rates denoted by colour (Figure 6c). As the roughness due to each treatment increases, sediment transport decreases, with the highest flow rate showing the most consistent reductions with increased roughness (Figure 6c).

One goal of this experiment was ultimately to determine the sediment reduction effects of erosion control treatments in roadside ditch lines using the concept of shear stress partitioning. To do so, we calculated—for each of the treatments—the total shear stress using the denominator of (8) and the grain shear stress using (9) solved for τ_g (Figure 7b). The merit of using shear stress partitioning to determine sediment reduction effects is well-illustrated by our data: The relationship between total shear stress and sediment transport is disjointed (Figure 7a). Despite a consistent increase in calculated total shear stress for different erosion control treatments, their associated sediment transport estimates were consistently lower than bare

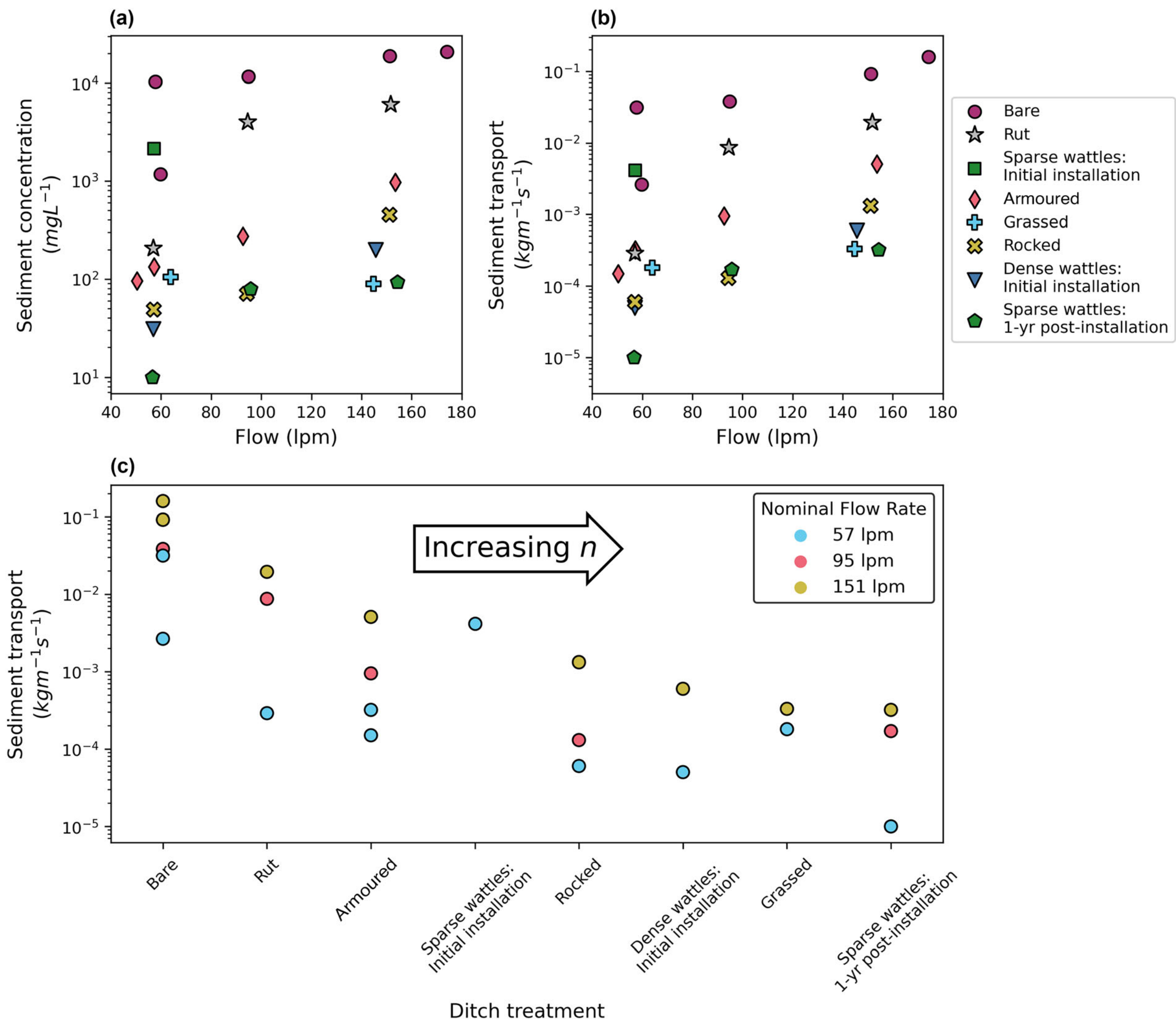

FIGURE 6 (a) Sediment concentration values for each ditch condition and their relationship to flow. (b) Sediment transport values for each ditch condition based on sediment concentration and flow width. (c) Strip plot showing the spread of sediment transport values for each ditch treatment. The nominal flow rates for each sediment transport value are denoted by different colours. [Color figure can be viewed at wileyonlinelibrary.com]

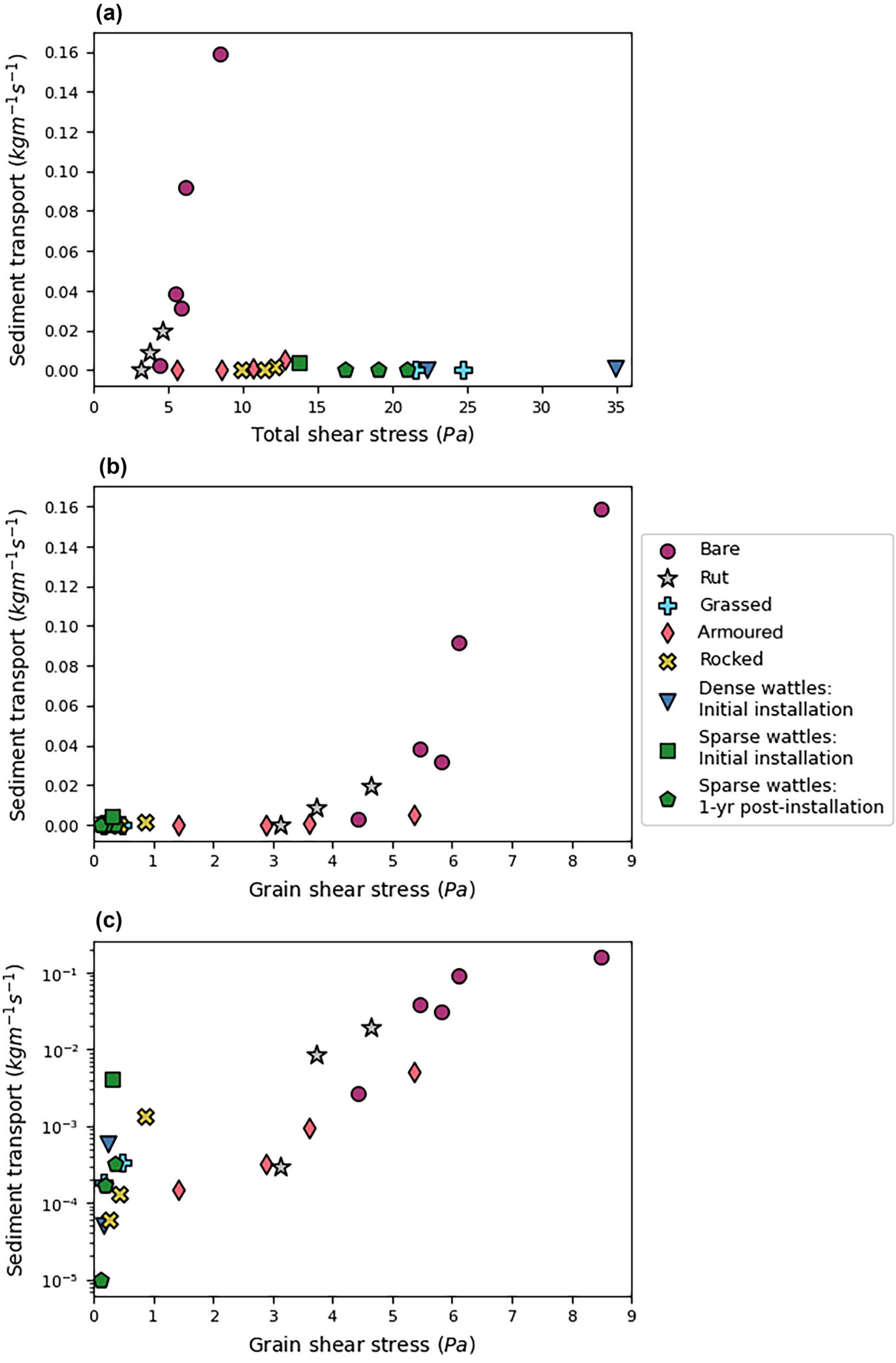

FIGURE 7 (a) Measured sediment transport values as a function of total shear stress, (b) measured sediment transport values as a function of grain shear stress, and (c) measured sediment transport values as a function of grain shear stress with a log-scale *y*-axis. [Color figure can be viewed at wileyonlinelibrary.com]

ditches and ruts (only under higher flow). This seemingly counterintuitive behaviour can only be explained when effective (grain) shear stress is used, organizing the data points consistently along a curve, where all the erosion control treatment sediment fluxes are now pushed back to consistently small values, largely less than 1 Pa, while bare plots remain constant ($\tau_g = \tau_t$). The relationship between grain shear stress and sediment transport aligns with the expectation that increased roughness results in decreased sediment transport (Figure 7b,c). Furthermore, if filtering were an additional effect of some erosion control treatments, sediment yield from filtering treatments (grass, initial installation of wattles, and rocking) might be systematically lower than the mean expectation based on the pattern of points (e.g., a fitted curve). No such pattern is observed in Figure 7c. As discussed above (Section 1), adding roughness elements to the ditch line (i.e., erosion control treatments) increases the total shear stress acting on the ditch due to the deepening and slowing of water flow. However, as also discussed previously, the resulting increase in friction around immobile roughness elements reduces the amount of grain shear stress available for sediment transport, which is illustrated by plotting total shear stress as a function of Manning's n due to additional roughness elements (Figure 1).

4.2 | Erosion control treatment effectiveness in context of climate

Because sediment transport is a strongly nonlinear function of grain shear stress, we must consider potential sediment yield reductions from treatments in the context of not just a few flows, as done with the field study. Rather, we should consider potential sediment yield reductions in the context of an ensemble of flows as might be seen over a season of runoff (e.g., Figure 4).

We can see that with higher roughness values, the exceedance probabilities of grain shear stress decrease in a relatively consistent nature (Figure 8a), with substantial reductions in the fraction of time that sediment would likely be transported. The d_{50} of soil aggregate particles in the field sites is approximately 1 mm, which has a relatively high critical shear stress based on Shield's criteria (0.566 Pa) as compared with the distribution of grain shear stresses estimated from observed flows and, as such, only yields modelled sediment transport for Manning's roughness values of up to 0.25 (Figure 8a). In Figures 4 and 8a, water flows (considered nonzero at a rate greater than 0.02 lpm) about 27% of the time, and in freshly disturbed ditches, grain shear stress exceeds the critical shear stress about 22% of the time (or about 80% of the time that water is flowing). In contrast, by increasing the roughness to $n = 0.10$ (armoured condition), runoff from the ditch would be expected to transport sediment only about 12% of the time (or 44% of the time there is runoff), and with $n = 0.25$ (rocked ditch), grain shear stress would exceed critical shear stress less than 2% of the time (or 7% of the time that runoff occurs). The fractional reduction in grain shear stress is constant for roughness values that do not vary with flow, whereas a slight decrease occurs for roughness values that linearly decrease with flow (Figure 8b).

From our calculated grain shear stresses, and using (12) in Section 2, we modelled the sediment transport capacity of ditch flow—when there was ditch flow—for different roughness values. The resulting sediment transport capacity exceedance probabilities decrease dramatically as a function of increasing roughness

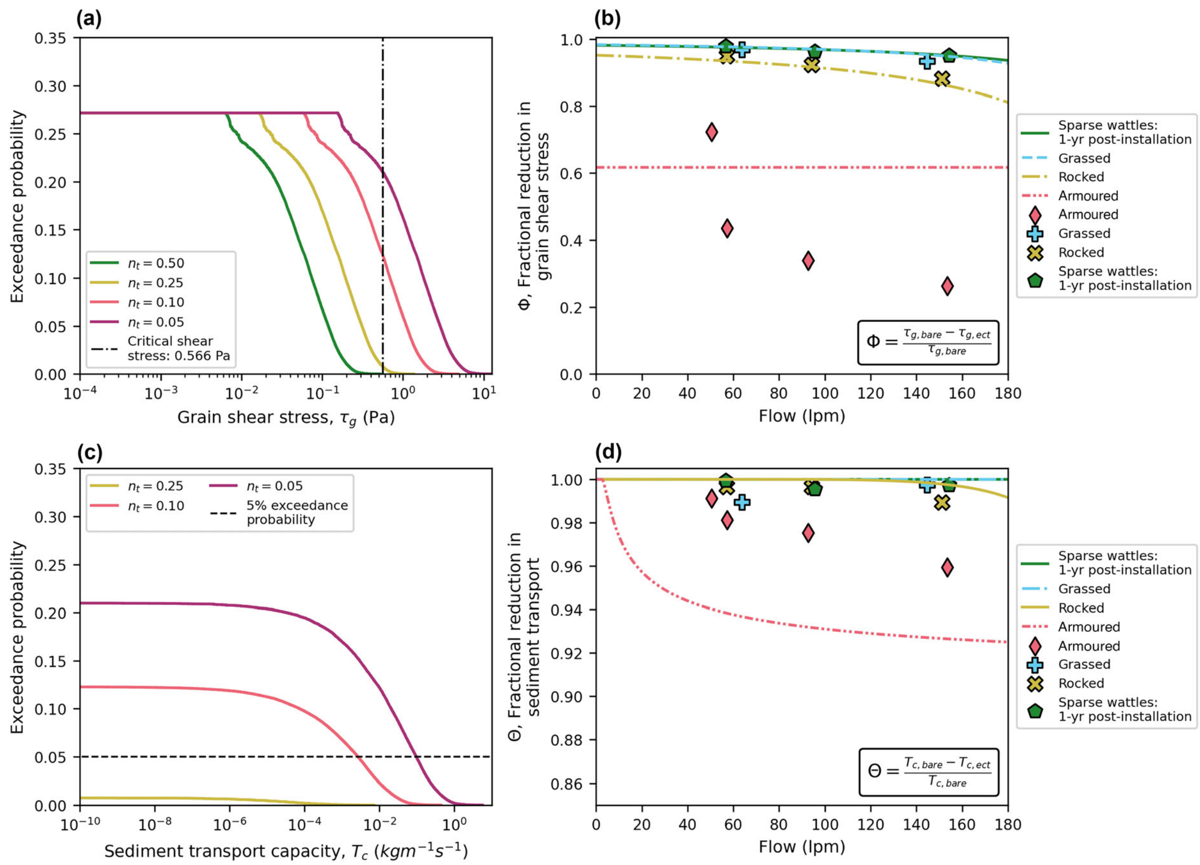

FIGURE 8 (a) Exceedance probabilities of grain shear stress, τ_g, for multiple n_t values calculated from (2) using observed ditch line flow hydrographs. Higher n_t values decrease grain shear stress. The critical shear stress threshold for a d_{50} of 1 mm is denoted by the vertical line. (b) Fractional reduction in grain shear stress, ϕ, for multiple ditch erosion control treatments. Erosion control treatments with n_t values that vary with flow provide less reduction in grain shear stress with higher flows. Experimental fractional reductions in grain shear stress are shown as points. (c) Exceedance probabilities of sediment transport capacity, T_c, for multiple n_t values. An exceedance probability of 5% is denoted by the horizontal line. (d) Theoretical fractional reduction in sediment transport capacity, θ, for multiple ditch erosion control treatments. Experimental fractional reductions in sediment transport are shown as points. [Color figure can be viewed at wileyonlinelibrary.com]

(Figure 8c). For 5% of the time (about 18 days per year), the transport capacity in a bare ditch ($n = 0.05$) would exceed 0.1 kg m^{-1} s^{-1}, a rate that is almost never expected to occur in an armoured ditch ($n = 0.10$). At the same time, in an armoured ditch, 5% of the time, transport capacity would be expected to exceed 0.002 kg m^{-1} s^{-1}, which is about 2% of the rate in a bare ditch for that exceedance probability. Integrating over the ensemble of flows, the bare ditch ($n = 0.05$) would have a transport capacity, T_c, of 61 Mg m^{-1}year^{-1}, an armoured ditch ($n = 0.10$) would have a T_c of 2.8 Mg m^{-1}year^{-1}, and the higher roughness of a rocked ditch ($n = 0.25$) would have a T_c of about 0.04 Mg m^{-1}year^{-1}. Actual erosion collected from a ditch would be smaller because available sediment would eventually be depleted, but the contrast in transport capacity integrated over the year gives a more concrete sense of the effect of added roughness on sediment yield. One notable point is that for low flows (common), a total roughness of $n = 0.10$ transitions from nearly complete reduction in sediment transport at 4 lpm or less to around 94% reduction at 57 lpm in a nonlinear way (Figure 8d). The modelled reductions are nearly 100% for a ditch with installed erosion control treatments (rocked ditch or stronger; $n \geq 0.25$). In other studies, measurements of sediment yield from road segments with recently disturbed versus armoured ditches over a few months to years showed reductions ranging from 85% (Luce & Black, 1999, 2001b) to nearly complete reduction (Luce & Black, 2001a).

5 | DISCUSSION

Shear stress partitioning offers an effective way of characterizing the effect of forest road erosion control treatments in reducing sediment transport through the use of their associated Manning's roughness. Because Manning's roughness associated with shallow flow is typically an empirical value coming from limited studies with varying conditions and contexts and few, if any, studies use Manning's n to evaluate erosion control treatment effectiveness, comparing all our measured Manning's roughness values to the literature is challenging. Our measured roughness values for bare soil ($n \simeq 0.05$), grass ($n \simeq 0.45$ to 0.75), and a rocked surface ($n \simeq 0.25$ to 0.35) are reasonably consistent with previously established values for shallow flow (Figure 5; e.g., Arcement & Schneider, 1989; Barros & Colello, 2001; Emmett, 1970; Engman, 1986). While not comparable with established roughness values due to limited studies, wattles do show comparable roughness values to grass. Measuring the roughness of a ditch line erosion control treatment offers an efficient and more general way to estimate the effectiveness of a given erosion control treatment, when used in a sediment transport equation driven by discharge, for differing conditions and contexts.

This final point is important—99% of observed flows that were >0.02 lpm in this dataset were less than 57 lpm, and in this range of flows, there is a variable and nonlinear sensitivity of fractional sediment transport capacity reduction (θ) as a function of flow rate (Figure 8d). Any experiment that reports a fractional sediment reduction from a treatment equivalent to an armoured ditch would need to qualify that the reduction is applicable to the particular flow rate used, and any study integrating sediment over a season would need to report the ensemble probability distribution of precipitation or flow. Directly transferring a fractional reduction from a mild rainy climate (e.g., northwest United States and northern Europe) to one where high intensity storms are more common (e.g., tropics and southeast United States) or places where snowmelt is more common is not necessarily a reasonable expectation. The change in roughness associated with an erosion control treatment, however, should be transferable through the use of shear stress partitioning in a sediment transport model.

While most erosion control treatments maintained constant total roughness with varying flow, three erosion control treatments had roughness decrease as flow increased (Figure 5): rocking, grass, and 1 year-old wattles. Each of these treatments had unique physical characteristics that we hypothesize contribute to their decreasing relationship between roughness and flow (Figure 9).

For the site with a rocked ditch (approximately $d_{50} = 38$ mm), the decrease in roughness as flow increased can likely be attributed to the fraction of the cross-sectional area of flow navigating the immobile roughness elements. With low flow, the majority of the water is moving through the subsurface (the interstitial spaces between the rocks) of the channel, with minimal surface flow (Figure 9a). As the flow increases, the fraction of the water being slowed due to immobile roughness elements decreases (e.g., Barros & Colello, 2001; Chen et al., 2015).

For the grassed site, the decrease in roughness with higher flows is similar to the rocked site: a decrease in the fraction of the cross-sectional area of flow experiencing immobile elements, but due to different mechanics. With lower flows, the water must flow through grass and vegetation stems. As the flow increases, the vegetation begins to bend, which effectively "smooths" these immobile roughness elements, causing the total roughness to decrease (Figure 9b; e.g., Chen et al., 2015; Jordanova & James, 2003; Nepf, 2012).

The decrease in roughness with an increase in flow for the 1 year-old sparse wattles site can likely be attributed to both the fraction of the cross-sectional area of flow navigating immobile roughness elements and the dam-and-reservoir effect seen during the experiment. The wattles at this site were initially installed in May 2020. During those initial wattle experimental runs, the flow never overtopped any of the wattles; rather, the flow went under or through the wattles (Figure 9c), which led to relatively consistent roughness values for varying flows. One year later, however, the wattles had not experienced any maintenance. Sediment and debris had built up inside of and behind each wattle, and, as such, the wattles acted like a series of dams and reservoirs (see Edwards et al., 2016). The initially high roughness values for the 1 year-old wattles can likely be attributed to the severe slowing of water as it built up behind each wattle before spilling over. As the flow increased, that slowing had less of an effect, and the fraction of the flow seeing the immobile roughness element decreased (Figure 9d).

In conjunction with the roughness, the sediment concentration grab samples validated the use of shear stress partitioning to evaluate reduced sediment transport effects due to erosion control treatment installation. This is demonstrated by the relationship between measured sediment transport and total shear stress (Figure 7a) and measured sediment transport and grain shear stress (Figure 7b). The trend between sediment transport and grain shear stress (Figure 7c) indicates that the increase in flow roughness due to additional immobile elements is likely the key driver in the reduction of sediment transport, rather than other mechanisms, such as binding effects of vegetation roots or filtering by wattles (which leads to rapid clogging with little internally retained sediment in any event).

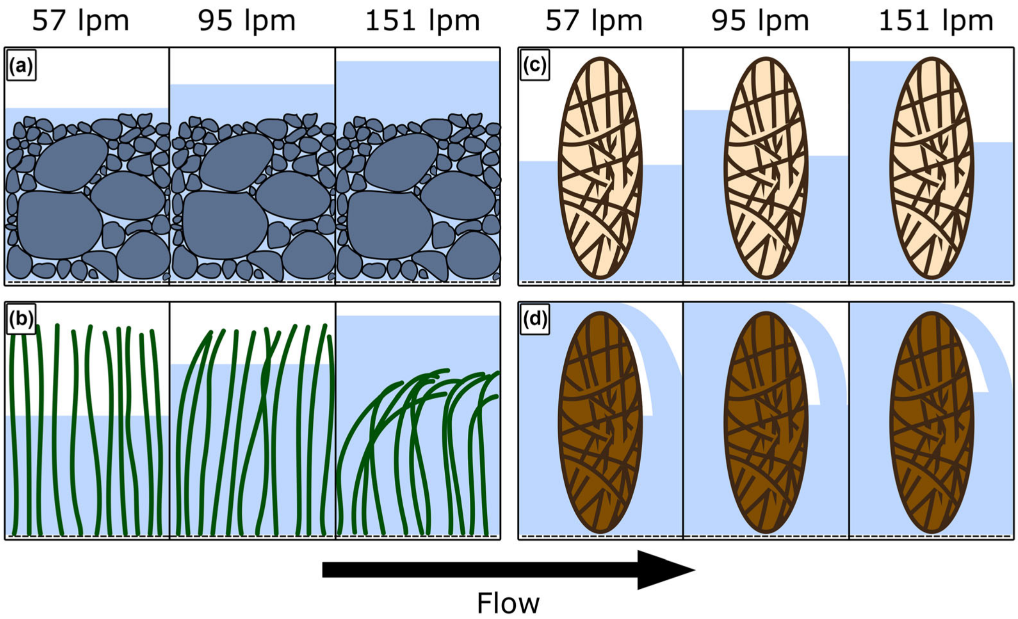

FIGURE 9 Drawings showing side views of the following: (a) The rocked ditch as flow increases. Once the flow gets to 151 lpm, the water far overtops the rocking, causing the fraction of the flow cross-sectional area being slowed by the immobile roughness to decrease. (b) The grassed ditch as flow increases. The highest flow causes the vegetation to bend, effectively smoothing the cross section. (c) The initial installation of straw wattles, where the flow went under or through the wattles, as they were brand new. (d) The wattles after they had been in the field for a year without any maintenance, causing them to become clogged with sediment. At all flow rates, the space behind the wattles fills up with water then overtops, producing a reservoir-and-dam effect, which slows the water down. [Color figure can be viewed at wileyonlinelibrary.com]

We estimated that a majority of ditch line erosion control treatments decreased calculated grain shear stress, and therefore modelled sediment transport, by almost 100%, producing fractional reductions near 1 (Figure 8d). In terms of measured sediment transport, we found that all treatments in our experimental runs produced some amount of sediment transport, including those with high roughness values. One site had a higher-than-expected sediment concentration value: sparse wattles during the initial installation (Figure 6). In the case of the sparse wattle initial installation, the measured sediment concentration value is high likely due to three factors: (1) The small amount of ditch below the final wattle had some erosion; (2) the ditch in which the wattles were installed had been recently disturbed and therefore had a larger amount of easily accessible sediment for transport; and (3) the wattles had a tendency to slightly float immediately after installation and, again, had a larger amount of easily accessible sediment for transport. Additionally, the sparse wattle installation had enough space between wattles that erosion and suspension of fine material was possible therein, especially at lower flows. Indeed, the spatial heterogeneity in grain shear stress is not fully accounted for in our modelling approach, which assumes uniform roughness and grain shear stress.

Overall, the decrease in measured sediment transport and calculated sediment transport capacities with erosion control treatment installation emphasizes the importance of ditch line erosion control treatment installation both from the perspective of ditch erosion reduction and potential mitigation of sediment transport from other elements within the road prism. Erosion control treatment installation can help reduce large ditch line erosion events, particularly immediately after road ditch grading (e.g., Luce & Black, 2001b) or new road construction (e.g., Megahan, 1974). Additionally, roads that are crowned or insloped allow for sediment from the road surface to travel to the ditch line where erosion control treatments can mitigate the tread-derived sediment. However, due to traffic and road deformation, wheel ruts tend to form on the road surface, which can cause water and sediment to bypass ditch line erosion control treatments (Alvis et al., 2023). As discussed above, a rut on the road (Figure 2b) has a similar roughness to a bare (recently disturbed) ditch and therefore has a high likelihood of carrying sediment in its rill-like flow. The interaction between the ditch line and other elements of the road prism is more complex and requires further exploration.

While the results from our experiment are promising, we have a limited number of observations for a limited number of erosion control treatments. However, we are not in the realm of conjecture, as both ample theory and empirical evidence exist for estimating the link between added roughness and sediment mobility and transport (e.g., Kothyari et al., 2009; Prosser et al., 1995; Thompson et al., 2004). Geomorphologically, both shear stress partitioning and the relationship between roughness and sediment transport are commonly utilized to estimate erosion and sedimentation in rivers and on vegetated hillslopes (e.g., Darby et al., 2010; Ferguson et al., 2019; Istanbulluoglu & Bras, 2005; Li, Venditti, et al., 2022). Regardless, future studies to empirically validate the relationship between roughness measurements and ditch line erosion control treatment sediment reduction, especially for a larger range of contexts and conditions, are warranted.

6 | CONCLUSION

Using the notion that the additional roughness of ditch line erosion control treatments can be used to examine their effectiveness—in conjunction with existing theory surrounding shear stress partitioning—we evaluated several ditch line erosion control treatments. We found that (1) each erosion control treatment yielded consistent Manning's *n* values across multiple replications and sites, with a bare ditch (no treatment) having the lowest roughness ($n = 0.05$) and a densely wattled ditch having the highest roughness ($n = 0.75$); (2) when combined from each experiment, the sediment load and calculated grain shear stress data yielded a single positive relationship, which suggests the effect of additional roughness on grain shear stress is a main driver in the reduction of ditch line sediment load; and (3) our data demonstrated that fractional erosion reduction had a variable and nonlinear sensitivity to low flow rates (99% of observed flows) for lower roughnesses, which emphasizes the importance of context (i.e., climate and other conditions) in terms of fractional erosion reduction for a given treatment.

In contrast to the fixed sediment reductions determined through traditional engineering trials, the use of Manning's *n* and relevant established theory can allow for more rigorous extrapolation to other contexts and climates. Our study demonstrated that Manning's *n*, in tandem with shear stress partitioning in a sediment transport model, can be used in such a way for a few conditions and contexts. However, further research should be done to establish the use of roughness as a physical metric to evaluate erosion control treatment effectiveness for a wider range of conditions and contexts. Additionally, being able to characterize erosion control treatments with continuous numerical values would also pave the way for later empirical testing of the effect of additional ditch line roughness on overall road segment sediment production.

AUTHOR CONTRIBUTIONS

Conceptualization: Amanda D. Alvis, Charles H. Luce, Erkan Istanbulluoglu, Thomas Black, Julie Dieu, and Jenelle Black. *Data curation*: Amanda D. Alvis, Charles H. Luce, Thomas Black, and Jenelle Black. *Formal analysis*: Amanda D. Alvis, Charles H. Luce, Erkan Istanbulluoglu, and Thomas Black. *Funding acquisition*: Amanda D. Alvis, Charles H. Luce, Erkan Istanbulluoglu, Thomas Black, Julie Dieu, and Jenelle Black. *Investigation*: Amanda D. Alvis, Charles H. Luce, Erkan Istanbulluoglu, Thomas Black, Julie Dieu, and Jenelle Black. *Methodology*: Amanda D. Alvis, Charles H. Luce, Erkan Istanbulluoglu, Thomas Black, Julie Dieu, and Jenelle Black. *Project administration*: Charles H. Luce, Thomas Black, and Julie Dieu. *Resources*: Amanda D. Alvis, Charles H. Luce, Erkan Istanbulluoglu, Thomas Black, Julie Dieu, and Jenelle Black. *Software*: Amanda D. Alvis and Charles H. Luce. *Supervision*: Charles H. Luce, Erkan Istanbulluoglu, Thomas Black, and Julie Dieu. *Validation*: Amanda D. Alvis and Thomas Black. *Visualization*: Amanda D. Alvis and Charles H. Luce. *Writing—original draft preparation*: Amanda D. Alvis, Charles H. Luce, and Erkan Istanbulluoglu. *Writing—review and editing*: Amanda D. Alvis, Charles H. Luce, Erkan Istanbulluoglu, Thomas Black, Julie Dieu, and Jenelle Black.

ACKNOWLEDGEMENTS

This research was made possible by public funding through the Cooperative Monitoring, Evaluation, and Research (CMER) Committee within the Washington State Department of Natural Resources Adaptive Management Program. The authors thank Sam Calahan, Lauren Wittkopf, Bob Danehy, and Teresa Miskovic for helping with field data collection and Alexander Prescott for helping with field data collection and logistical support.

CONFLICT OF INTEREST STATEMENT

The authors declare that there are no competing interests.

DATA AVAILABILITY STATEMENT

The data presented in this manuscript are not currently publicly available due to an agreement with the Cooperative Monitoring, Evaluation, and Research (CMER) Committee within the Washington State Department of Natural Resources Adaptive Management Program but are available from the corresponding author upon reasonable request and approval from CMER. Additionally, the data will be made publicly available in the future upon completion of the overarching project and CMER's approval of the final report.

ORCID

Amanda D. Alvis https://orcid.org/0000-0002-9662-1121

REFERENCES

Al-Hamdan, O.Z., Pierson, F.B., Nearing, M.A., Williams, C.J., Stone, J.J., Kormos, P.R., et al. (2013) Risk assessment of erosion from concentrated flow on rangelands using overland flow distribution and shear stress partitioning. *Transactions of the ASABE*, 56(2), 539–548. Available from: https://doi.org/10.13031/2013.42684

Al-Hamdan, O.Z., Pierson, F.B., Robichaud, P., Elliot, W.J. & Williams, C.J. (2022) New erodibility parameterization for applying WEPP on rangelands using ERMiT. *Journal of the ASABE*, 65(2), 251–264. Available from: https://doi.org/10.13031/ja.14564

Alvis, A.D., Luce, C.H. & Istanbulluoglu, E. (2023) How does traffic affect erosion of unpaved forest roads? *Environmental Reviews*, 31(1), 182–194. Available from: https://doi.org/10.1139/er-2022-0032

Arcement, G.J. & Schneider, V.R. (1989) *Guide for selecting Manning's roughness coefficients for natural channels and flood plains*. USGS Numbered Series 2339. Washington, D.C.: U.S. Geological Survey. Available from: https://doi.org/10.3133/wsp2339.

Aust, W.M., Bolding, M.C. & Barrett, S.M. (2015) Best management practices for low-volume forest roads in the Piedmont region: summary and implications of research. *Transportation Research Record*, 2472(1), 51–55. Available from: https://doi.org/10.3141/2472-06

Barros, A.P. & Colello, J.D. (2001) Surface roughness for shallow overland flow on crushed stone surfaces. *Journal of Hydraulic Engineering*, 127(1), 38–52. Available from: https://doi.org/10.1061/(ASCE)0733-9429(2001)127:1(38

Boston, K. (2016) The potential effects of forest roads on the environment and mitigating their impacts. *Current Forestry Reports*, 2(4), 215–222. Available from: https://doi.org/10.1007/s40725-016-0044-x

Buffington, J.M. & Montgomery, D.R. (1997) A systematic analysis of eight decades of incipient motion studies, with special reference to gravel-bedded rivers. *Water Resources Research*, 33(8), 1993–2029. Available from: https://doi.org/10.1029/96WR03190

Burroughs, E.R. & King, J.G. (1989) *Reduction of soil erosion on forest roads*. Ogden, UT: U.S. Department of Agriculture, Forest Service, Intermountain Research Station Available from: 10.2737/INT-GTR-264.

Burroughs, E.R., Watts, F.J., King, J.G., Haber, D.F., Hansen, D. & Flerchinger, G. (1984) Relative effectiveness of rocked roads and ditches in reducing surface erosion. In: *21st Annual Engineering, Geology, and Soils Engineering Symposium*. Moscow, ID: University of Idaho, pp. 251–263.

Cartwright, N. (2007) Are RCTs the gold standard? *BioSocieties*, 2(1), 11–20. Available from: https://doi.org/10.1017/S1745855207005029

Chen, Y., Xing-nian, L. & Xie-kang, W. (2015) Effects of roughness elements distribution on overland flow resistance. *Journal of Mountain Science*, 12(5), 1145–1156. Available from: https://doi.org/10.1007/s11629-014-3391-8

Collins, L.M. & Johnston, C.E. (1995) Effectiveness of straw bale dams for erosion control in the Oakland Hills following the fire of 1991. In: Keeley, J.E. & Scott, T. (Eds.) *Brushfires in California wildlands: ecology and resource management*. Fairfield, WA: International Association of Wildland Fire, pp. 171–183.

Cristan, R., Aust, W.M., Bolding, M.C. & Barrett, S.M. (2019) Estimated sediment protection efficiencies for increasing levels of best management practices on forest harvests in the Piedmont, USA. *Forests*, 10(11), 997. Available from: https://doi.org/10.3390/f10110997

Cristan, R., Aust, W.M., Bolding, M.C., Barrett, S.M., Munsell, J.F. & Schilling, E. (2016) Effectiveness of forestry best management practices in the United States: literature review. *Forest Ecology and Management*, 360, 133–151. Available from: https://doi.org/10.1016/j.foreco.2015.10.025

Dangle, C.L., Bolding, M.C., Aust, W.M., Barrett, S.M. & Schilling, E.B. (2019) Best management practices influence modeled erosion rates at forest haul road stream crossings in Virginia. *JAWRA Journal of the American Water Resources Association*, 55(5), 1169–1182. Available from: https://doi.org/10.1111/1752-1688.12762

Darby, S.E., Trieu, H.Q., Carling, P.A., Sarkkula, J., Koponen, J., Kummu, M., et al. (2010) A physically based model to predict hydraulic erosion of fine-grained riverbanks: the role of form roughness in limiting erosion. *Journal of Geophysical Research*, 115(F4), F04003. Available from: https://doi.org/10.1029/2010JF001708

Donald, W.N., Zech, W.C., Fang, X. & LaMondia, J.J. (2013) Evaluation of wheat straw wattles for velocity reduction in ditch check installations. *Transportation Research Record: Journal of the Transportation Research Board*, 2358(1), 69–78. Available from: https://doi.org/10.3141/2358-08

Edwards, P.J., Wood, F. & Quinlivan, R.L. (2016) *Effectiveness of best management practices that have application to forest roads*. General Technical Report NRS-163. Parsons, West Virginia, USA: USDA Forest Service Northern Research Station.

Einstein, H.A. & Banks, R.B. (1950) Fluid resistance of composite roughness. *Transactions of the American Geophysical Union*, 31(4), 603–610. Available from: https://doi.org/10.1029/TR031i004p00603

Einstein, H.A. & Barbarossa, N.L. (1952) River channel roughness. *Transactions of the American Society of Civil Engineers*, 117(1), 1121–1132. Available from: https://doi.org/10.1061/TACEAT.0006666

Emmett, W.W. (1970) *The hydraulics of overland flow on hillslopes*. Report 662A. Washington, D.C.: U.S. Government Publishing Office. Available from: https://doi.org/10.3133/pp662A

Engman, E.T. (1986) Roughness coefficients for routing surface runoff. *Journal of Irrigation and Drainage Engineering*, 112(1), 39–53. Available from: https://doi.org/10.1061/(ASCE)0733-9437(1986)112:1(39

Ferguson, R.I., Hardy, R.J. & Hodge, R.A. (2019) Flow resistance and hydraulic geometry in bedrock rivers with multiple roughness length scales. *Earth Surface Processes and Landforms*, 44(12), 2437–2449. Available from: https://doi.org/10.1002/esp.4673

Foster, G.R., Lane, L.J., Nearing, M.A., Finkner, S.C. & Flanagan, D.C. (1989) Erosion component. In: Lane, L.J. & Nearing, M.A. (Eds.) *USDA-water erosion prediction project: hillslope profile model documentation*. West Lafayette, IN: National Soil Erosion Research Lab (NSERL Report, 2), pp. 1–12.

Govers, G. (1992) Evaluation of transporting capacity formulae for overland flow. In: *Overland flow: hydraulics and erosion mechanics*. New York: Chapman and Hall, pp. 243–273.

Istanbulluoglu, E. & Bras, R.L. (2005) Vegetation-modulated landscape evolution: effects of vegetation on landscape processes, drainage density, and topography. *Journal of Geophysical Research*, 110(F2), F02012. Available from: https://doi.org/10.1029/2004JF000249

Istanbulluoglu, E., Tarboton, D.G., Pack, R.T. & Luce, C. (2002) A probabilistic approach for channel initiation. *Water Resources Research*, 38(12), 61-1–61-14. Available from: https://doi.org/10.1029/2001WR000782

Istanbulluoglu, E., Tarboton, D.G., Pack, R.T. & Luce, C. (2003) A sediment transport model for incision of gullies on steep topography. *Water Resources Research*, 39(4), 1103. Available from: https://doi.org/10.1029/2002WR001467

Jordanova, A.A. & James, C.S. (2003) Experimental study of bed load transport through emergent vegetation. *Journal of Hydraulic Engineering*, 129(6), 474–478. Available from: https://doi.org/10.1061/(ASCE)0733-9429(2003)129:6474

Kemper, W.D. & Rosenau, R.C. (1986) Aggregate stability and size distribution. In: Klute, A. (Ed.) *Methods of soil analysis*. Madison, WI: American Society of Agronomy-Soil Science Society of America, pp. 425–442. Available from: https://doi.org/10.2136/sssabookser5.1.2ed.c17

Kothyari, U.C., Hashimoto, H. & Hayashi, K. (2009) Effect of tall vegetation on sediment transport by channel flows. *Journal of Hydraulic Research*, 47(6), 700–710. Available from: https://doi.org/10.3826/jhr.2009.3317

Lane, S.N. (2014) Acting, predicting and intervening in a socio-hydrological world. *Hydrology and Earth System Sciences*, 18(3), 927–952. Available from: https://doi.org/10.5194/hess-18-927-2014

Laursen, E.M. (1958) The total sediment load of streams. *Journal of the Hydraulics Division*, 84(1), 1–36. Available from: https://doi.org/10.1061/JYCEAJ.0000158

Le Bouteiller, C. & Venditti, J.G. (2015) Sediment transport and shear stress partitioning in a vegetated flow. *Water Resources Research*, 51(4), 2901–2922. Available from: https://doi.org/10.1002/2014WR015825

Li, L., Nearing, M.A., Polyakov, V.O., Nichols, M.H., Pierson, F.B. & Cavanaugh, M.L. (2020) Evolution of rock cover, surface roughness, and its effect on soil erosion under simulated rainfall. *Geoderma*, 379, 114622. Available from: https://doi.org/10.1016/j.geoderma.2020.114622

Li, T., Venditti, J.G., Rennie, C.D. & Nelson, P.A. (2022) Bed and bank stress partitioning in bedrock rivers. *Journal of Geophysical Research - Earth Surface*, 127(2), e2021JF006360.

Li, X., Zhang, Y., Ji, X., Strauss, P. & Zhang, Z. (2022) Effects of shrub-grass cover on the hillslope overland flow and soil erosion under simulated rainfall. *Environmental Research*, 214(Pt 1), 113774. Available from: https://doi.org/10.1016/j.envres.2022.113774

Likitlersuang, S., Kounyou, K. & Prasetyaningtiyas, G.A. (2020) Performance of geosynthetic cementitious composite mat and vetiver on soil erosion control. *Journal of Mountain Science*, 17(6), 1410–1422. Available from: https://doi.org/10.1007/s11629-019-5926-5

Luce, C.H. & Black, T.A. (1999) Sediment production from forest roads in western Oregon. *Water Resources Research*, 35(8), 2561–2570. Available from: https://doi.org/10.1029/1999WR900135

Luce, C.H. & Black, T.A. (2001a) Effects of traffic and ditch maintenance on forest road sediment production. In: *Proceedings of the Seventh Federal Interagency Sedimentation Conference*. Nevada: Reno, pp. V67–V74.

Luce, C.H. & Black, T.A. (2001b) *Spatial and temporal patterns in erosion from forest roads*. Land use and watersheds: Human influence on hydrology and geomorphology in urban and forest areas, pp. 165–178.

Manga, M. & Kirchner, J.W. (2000) Stress partitioning in streams by large woody debris. *Water Resources Research*, 36(8), 2373–2379. Available from: https://doi.org/10.1029/2000WR900153

Megahan, W.F. (1974) *Erosion over time on severely disturbed granitic soils: a model*. Research Paper INT-156. Ogden, Utah: U.S.: Department of Agriculture Forest Service Intermountain Forest and Range Experiment Station, p. 20.

Megahan, W.F., Wilson, M. & Monsen, S.B. (2001) Sediment production from granitic cutslopes on forest roads in Idaho, USA. *Earth Surface Processes and Landforms*, 26(2), 153–163. Available from: https://doi.org/10.1002/1096-9837(200102)26:2<153::AID-ESP172>3.0.CO;2-0

Moore, R.D. (2005) Slug injection using salt in solution. *Streamline Watershed Management Bulletin*, 8(2), 1–6.

Moore, I.D. & Burch, G.J. (1986) Sediment transport capacity of sheet and rill flow: application of unit stream power theory. *Water Resources Research*, 22(8), 1350–1360. Available from: https://doi.org/10.1029/WR022i008p01350

Nearing, M.A., Foster, G.R., Lane, L.J. & Finkner, S.C. (1989) A process-based soil erosion model for USDA-water erosion prediction project technology. *Transactions of ASAE*, 32(5), 1587–1593. Available from: https://doi.org/10.13031/2013.31195

Nepf, H.M. (2012) Flow and transport in regions with aquatic vegetation. *Annual Review of Fluid Mechanics*, 44(1), 123–142. Available from: https://doi.org/10.1146/annurev-fluid-120710-101048

PRISM Climate Group. (2023) *Oregon State University*, https://prism.oregonstate.edu, data created 7 Feb 2023, accessed 7 Feb 2023.

Prosser, I.P., Dietrich, W.E. & Stevenson, J. (1995) Flow resistance and sediment transport by concentrated overland flow in a grassland valley. *Geomorphology*, 13(1–4), 71–86. Available from: https://doi.org/10.1016/0169-555X(95)00020-6

Schussler, J.C., Kazaz, B., Perez, M.A., Blake Whitman, J. & Cetin, B. (2021) Field evaluation of wattle and silt fence ditch checks. *Transportation Research Record: Journal of the Transportation Research Board*, 2675(6), 281–293. Available from: https://doi.org/10.1177/0361198121992073

Sojka, R.E., Bjorneberg, D.L., Entry, J.A., Lentz, R.D. & Orts, W.J. (2007) Polyacrylamide in agriculture and environmental land management. In: Sparks, D.L. (Ed.) *Advances in agronomy*. United States: Academic Press Inc., pp. 75–162. Available from: https://doi.org/10.1016/S0065-2113(04)92002-0

Thompson, A.M., Wilson, B.N. & Hansen, B.J. (2004) Shear stress partitioning for idealized vegetated surfaces. *Transactions of ASAE*, 47(3), 701–709. Available from: https://doi.org/10.13031/2013.16102

Tiscareno-Lopez, M., Lopes, V.L., Stone, J.J. & Lane, L.J. (1994) Sensitivity analysis of the WEPP watershed model for rangeland applications II: channel processes. *Transactions of ASAE*, 37(1), 151–158. Available from: https://doi.org/10.13031/2013.28065

Tollner, E.W., Barfield, B.J., Vachirakornwatana, C. & Haan, C.T. (1977) Sediment deposition patterns in simulated grass filters. *Transactions of ASAE*, 20(5), 0940–0944. Available from: https://doi.org/10.13031/2013.35679

United States Bureau of Reclamation. (2001) '*Water measurement manual*'. Washington, D.C.: U.S. Government Printing Office. Available at: http://www.usbr.gov/tsc/techreferences/mands/wmm/ (Accessed: 7 September 2023).

Whitman, J.B., Schussler, J.C., Perez, M.A. & Liu, L. (2021) Hydraulic performance evaluation of wattles used for erosion and sediment control. *Journal of Irrigation and Drainage Engineering*, 147(7), 04021028. Available from: https://doi.org/10.1061/(ASCE)IR.1943-4774.0001586

Wright, K.N. (2010) *Evaluation of check dams for sediment control on disturbed land surfaces*. M.S. Thesis. Urbana, IL: University of Illinois at Urbana-Champaign.

Yager, E.M., Kirchner, J.W. & Dietrich, W.E. (2007) Calculating bed load transport in steep boulder bed channels. *Water Resources Research*, 43(7), W07418. Available from: https://doi.org/10.1029/2006WR005432

Yetemen, O., Saco, P.M. & Istanbulluoglu, E. (2019) Ecohydrology controls the geomorphic response to climate change. *Geophysical Research Letters*, 46(15), 8852–8861. Available from: https://doi.org/10.1029/2019GL083874

How to cite this article: Alvis, A.D., Luce, C.H., Istanbulluoglu, E., Black, T., Dieu, J. & Black, J. (2024) Using additional roughness to characterize erosion control treatment effectiveness in roadside ditch lines. *Earth Surface Processes and Landforms*, 49(4), 1255–1272. Available from: https://doi.org/10.1002/esp.5763

APPENDIX A: SHEAR STRESS PARTITIONING RATIOS

As discussed in Section 2.1 of the main text, Einstein and Barbarossa (1952) proposed to partition shear stress into various components such as the shear stress that acts upon sediment grains and the shear stress that acts upon forms in the channel (e.g., bed forms and vegetation).

$$\tau_t = \rho_w g R S, \tag{A1}$$

$$\tau_t = \tau_g + \tau_a, \tag{A2}$$

where τ_g is the grain shear stress and τ_a is the additional shear stress. ρ_w is the density of water, g is the acceleration due to gravity, R is the hydraulic radius, and S is the channel slope.

In this appendix, we take this knowledge and look at the partitioning ratio of grain shear stress to total bed shear stress (Section 2.1 and Equation 2) using different approximations.

A.1 | General form with velocity term

Starting with Manning's equation and rearranging, we can obtain the hydraulic radius, R, of the channelized flow as a function of flow velocity, U, roughness, n, and slope, S:

$$U = \frac{R^{2/3} S^{1/2}}{n} \ (Manning),$$

$$\Rightarrow R = \left(n \frac{U}{S^{1/2}}\right)^{3/2}. \tag{A3}$$

Following the logic of Laursen (1958), Equation (A3) can be used for obtaining the grain component hydraulic radius, R_g, given an average flow velocity in the channel:

$$R_g = \left(n_g \frac{U}{S^{1/2}}\right)^{3/2}, \tag{A4}$$

where n_g is the grain roughness.

In the same form as Equation (A1), the effective shear stress acting on the grains, τ_g, can be written as

$$\tau_g = \rho_w g R_g S,$$

$$\tau_g = \rho_w g n_g^{3/2} U^{3/2} S^{1/4}, \tag{A5}$$

where ρ_g is the density of water and g is the acceleration of gravity.

For the shear stress partitioning ratio ($f_g = \frac{\tau_g}{\tau_t}$), we combine Equations (A1), (A3), and (A5) to get

$$\frac{\tau_g}{\tau_t} = \frac{n_g^{3/2} \rho_w g U^{3/2} S^{1/4}}{n_t^{3/2} \rho_w g U^{3/2} S^{1/4}},$$

$$\frac{\tau_g}{\tau_t} = \left(\frac{n_g}{n_t}\right)^{3/2}. \tag{A6}$$

Using this standard form of shear stress partitioning ratio maintains a dependency on constant velocity, and the resulting shear stress partitioning ratio is proportional to the ratio of grain roughness to total roughness raised to the 1.5 power.

A.2 | General form with no velocity term

In this subsection, we take the general form of the shear stress partitioning ratio and remove the dependency on constant velocity to get the equation in terms of fewer dependent variables. To do so, we write velocity as $U = \frac{Q}{A}$ and substitute in $A = \frac{R^2}{C^2}$ (sensu Istanbulluoglu et al., 2003; Moore & Burch, 1986), where C is a constant that is based on channel shape:

$$U = \frac{QC^2}{R^2}. \tag{A7}$$

Using these substitutions, we can rewrite Manning's equation for Q and solve for R:

$$Q = \frac{1}{nC^2} R^{8/3} S^{1/2},$$

$$\Rightarrow R = \left[\frac{nC^2}{S^{1/2}}\right]^{3/8} Q^{3/8}. \tag{A8}$$

Again, following the logic of Laursen (1958), R can be written for grain or total roughness as

$$R_g = \left[\frac{n_g C^2}{S^{1/2}}\right]^{3/8} Q^{3/8},$$

$$R_t = \left[\frac{n_t C^2}{S^{1/2}}\right]^{3/8} Q^{3/8}. \tag{A9}$$

Recalling Equation (A7), we can now express U as a function of Q, n, and S:

$$U = \frac{C^{1/2}}{n^{3/4}} Q^{1/4} S^{3/8}. \tag{A10}$$

We now have all the pieces needed to calculate the shear stress partitioning ratio. From Equation (A2) and Manga and Kirchner (2000), we have

$$\tau_t = \tau_g + \tau_a,$$

$$\rho_w g R_t S = \rho_w C_{dg} U^2 + \rho_w C_{da} U^2,$$

or

$$\rho_w g R_t S = \rho_w C_{dt} U^2, \tag{A11}$$

where $C_{dt} = C_{dg} + C_{da}$. And for bare conditions, we have

$$\tau_t = \tau_g,$$

$$\rho_w g R_g S = \rho_w C_{dg} U^2, \tag{A12}$$

which we can use to solve for C_{dg} (and C_{dt}):

$$C_{dg} = \frac{g R_g S}{U^2}. \tag{A13}$$

Substituting Equations (A9) and (A10):

$$C_{dg} = \frac{g\left[\frac{n_g C^2}{S^{1/2}}\right]^{3/8} Q^{3/8} S}{\left[\frac{C^{1/2}}{n_g^{3/4}} Q^{1/4} S^{3/8}\right]^2},$$

$$C_{dg} = \frac{g\left[\frac{n_g^{3/8} C^{3/4}}{S^{3/16}}\right] Q^{3/8} S}{\frac{C}{n_g^{3/2}} Q^{1/2} S^{3/4}},$$

$$C_{dg} = g n_g^{15/8} C^{-1/4} Q^{-1/8} S^{1/16}. \tag{A14}$$

And it follows that C_{dt} takes on the same form:

$$C_{dt} = n_t^{15/8} C^{-1/4} Q^{-1/8} S^{1/16} g. \tag{A15}$$

Our shear stress partitioning ratio, then, is

$$\frac{\tau_g}{\tau_t} = \frac{\rho_w g n_g^{15/8} C^{-1/4} Q^{-1/8} S^{1/16} U^2}{\rho_w g n_t^{15/8} C^{-1/4} Q^{-1/8} S^{1/16} U^2},$$

$$\frac{\tau_g}{\tau_t} = \left(\frac{n_g}{n_t}\right)^{15/8}. \tag{A16}$$

The resulting shear stress partitioning ratio here is proportional to the ratio of grain roughness to total roughness raised to the 1.875 power.

A.3 | Parabolic channel approximation with reduced dimensionality

In this subsection, we again take the general form of the shear stress partitioning ratio and remove the dependency on constant velocity to get the equation in terms of fewer dependent variables. Additionally, we use a parabolic approximation to further reduce the required variables.

In this case, we will follow a similar set of steps to Section A.2, but instead of using $A = \frac{R^2}{C^2}$ to calculate A, we instead use two simplifications: one for a parabolic channel's area, A, and one for the parabolic approximation of wetted perimeter, P, and hydraulic radius, R, assuming that the shape of water flow is wide and shallow:

$$A = \frac{a}{6} w^3, \tag{A17}$$

$$P \approx w, \tag{A18}$$

$$R = \frac{A}{P} \approx \frac{a}{6} w^2, \tag{A19}$$

where a is the parameter that determines the shape of a parabola and w is the top width of the channel flow.

We can substitute $w =$ into Equation (A17):

$$A = \frac{a}{6}\left(\frac{6}{a} R\right)^{3/2},$$

$$A = \sqrt{\frac{6}{a}} R^{3/2}, \tag{A20}$$

which we can substitute into Manning's equation and solve for R:

$$Q = \frac{1}{n}\sqrt{\frac{6S}{a}} R^{3/2} R^{2/3} = \frac{1}{n}\sqrt{\frac{6S}{a}} R^{13/6}, \tag{A21}$$

$$\Rightarrow R = \left(\frac{nQ}{\sqrt{\frac{6S}{a}}}\right)^{6/13}. \tag{A22}$$

Plugging Equation (A22) back into Equation (A20) to get A in terms of n, Q, S, and a:

$$A = \sqrt{\frac{6}{a}}\left(\frac{nQ}{\sqrt{\frac{6S}{a}}}\right)^{6/13*3/2} = \sqrt{\frac{6}{a}}\left(\frac{nQ}{\sqrt{\frac{6S}{a}}}\right)^{9/13}. \tag{A23}$$

Getting the velocity, U, in the same terms:

$$U = \frac{Q}{A} = Q\sqrt{\frac{a}{6}}\left(\frac{nQ}{\sqrt{\frac{6S}{a}}}\right)^{-9/13}. \tag{A24}$$

And calculating U^2 for ease of future arithmetic:

$$U^2 = Q^2 \frac{a}{6}\left(\frac{nQ}{\sqrt{\frac{6S}{a}}}\right)^{-18/13}$$

$$U^2 = \frac{Q^2 S^{9/13}\left(\frac{6}{a}\right)^{9/13}}{n^{18/13} Q^{18/13}\left(\frac{6}{a}\right)}. \tag{A25}$$

$$U^2 = \frac{Q^{8/13} S^{9/13}}{n^{18/13}\left(\frac{6}{a}\right)^{4/13}}$$

Following the logic of Section A.2 and using the forms of Equations (A12) through (A14), we can get C_{dg} in terms of n, Q, S, and a, too:

$$
\begin{aligned}
C_{dg} &= \frac{gR_gS}{U^2}\\
C_{dg} &= \frac{g\left(\frac{n_gQ}{\sqrt{\frac{6S}{a}}}\right)^{6/13}S}{\frac{Q^{8/13}S^{9/13}}{n_g^{18/13}\left(\frac{6}{a}\right)^{4/13}}}\\
C_{dg} &= \frac{gn_g^{6/13}Q^{6/13}Sn_g^{18/13}\left(\frac{6}{a}\right)^{4/13}}{Q^{8/13}S^{9/13}S^{3/13}\left(\frac{6}{a}\right)^{3/13}}\\
C_{dg} &= gn_g^{24/13}Q^{-2/13}S^{1/13}\left(\frac{6}{a}\right)^{1/13}
\end{aligned}
\qquad \text{(A26)}
$$

And it follows that C_{dt} takes on the same form:

$$C_{dt} = n_t^{24/13}Q^{-2/13}S^{1/13}\left(\frac{6}{a}\right)^{1/13}g. \qquad \text{(A27)}$$

Our shear stress partitioning ratio, then, is

$$
\begin{aligned}
\frac{\tau_g}{\tau_t} &= \frac{\rho_w g n_g^{24/13}Q^{-2/13}S^{1/13}\left(\frac{6}{a}\right)^{1/13}U^2}{\rho_w g n_t^{24/13}Q^{-2/13}S^{1/13}\left(\frac{6}{a}\right)^{1/13}U^2}\\
\frac{\tau_g}{\tau_t} &= \left(\frac{n_g}{n_t}\right)^{24/13}
\end{aligned}
\qquad \text{(A28)}
$$

The resulting shear stress partitioning ratio here is proportional to the ratio of grain roughness to total roughness raised to the 1.85 power.